DOI: 10.2478/s11696-011-0039-9

Impact of the type of anodic film formed and deposition time on the characteristics of porous anodic aluminium oxide films containing Ni metal

[a]Gaël Zamora, [a]Laurent Arurault*, [b]Peter Winterton, [a]René Bes

[a]*Bat 2R1,* [b]*Bat 4A, LCMIE, UPS/INPT/CNRS, CIRIMAT, Université de Toulouse, 118 route de Narbonne, 31062 Toulouse Cedex 9, France*

Porous anodic films containing nickel were prepared by AC electro-deposition. The porosity of the films was controlled by using different working conditions (anodisation electrolyte, voltage, and time). Then nickel was electro-deposited using an alternating voltage. The impact of the anodic film on the current density waveforms and the metal content can largely be explained by the porosity differences, while changing the deposition time caused changes due to over-oxidation of the aluminium substrate, experimentally proved by TEM. Finally, the impact of deposition time on the deposited metal was successfully fitted using an Elovich type law over a large time-span (up to 1800 s), showing the ability to achieve precise control of the metal content.

Keywords: aluminium, porous anodic film, metal AC electro-deposition

Introduction

The pioneering works on the electro-deposition of metals in porous anodic aluminium oxide films were reported in Italy in 1936 (Wernick et al., 1987). But its widespread use started in Japan after World War 2 for colouring purposes (Wernick et al., 1987). Then, new applications emerged for the first time in different fields such as magnetism (Kawai & Ueda, 1975), thermo-optics and dyeing (Anderson et al., 1980), catalysis (McBren & Moskovits, 1987), electronics (Preston & Moskovits, 1993), corrosion protection (Fukuda & Fukushima, 1982), and for antibacterial activity (Chi et al., 2002). Recently, the electro-deposition of metals in anodic films has acquired renewed interest due to the possibility of preparing nanodevices using porous templates based on anodic aluminium oxide films. The two main applications are in the preparation of metal nanorods from Au (Forrer et al., 2000; Wang et al., 2002), Ni (Nielsch et al., 2000; Yin et al., 2001; Jagminas et al., 2003), Bi (Yin et al., 2001), Cu, Co, Sn (Jagminas et al., 2003), Ag (Sauer et al., 2002), Fe (Yang et al., 2000)), or metal nanoparticles (Fe, Ni, Co) for the catalytic growth of carbon nanotubes (Kyotani et al., 1996; Papadopoulos et al., 2002) or for their magnetic properties (Wu et al., 2009).

Due to the presence of the compact (or barrier) layer at the bottom of the anodic films, electro-deposition cannot be performed using a direct electrical signal, current or voltage (Nielsch et al., 2000; Kallithrakas-Kontos et al., 1998; Yoo & Lee, 2004). Recent studies involving nanodevice preparation overcame this problem by drilling the barrier layer, facilitating the application of a direct electrical signal (Nielsch et al., 2000; Szkutnik et al., 2006; Hwang et al., 2005).

But, apart from nanodevice preparation, the usual applications require good corrosion resistance, i.e. to avoid perforation of the barrier layer. Thus, metal electro-deposition in the pores of the anodic films is generally performed using alternating or pulsed voltage (or sometimes current) (Lee et al., 1978, Zemanová et al., 2008a, 2008b, 2009a, 2009b; Arurault et al.,

*Corresponding author, e-mail: arurault@chimie.ups-tlse.fr

2010) to ensure renewal of the material in the confined volume of electrolyte contained in the mesopores.

The present study completes previous studies by our group (Salmi et al., 2000; Arurault & Bes, 2003, 2007; Arurault et al., 2004, 2006, 2010) which focused on the electro-deposition of nickel in porous anodic films on aluminium substrates, in order to prepare low-cost coloured articles. This work is more specifically concerned with the influence of the type of anodic film and the deposition time on the morphological characteristics of the coatings and the metal content in particular.

Experimental

The preparation process principally involved three successive steps: pre-treatment of surface, anodisation, and electrochemical deposition of nickel.

1050A (99.5 % Al) aluminium alloy sheet (60 mm × 40 mm × 1 mm) was degreased for one minute in an aqueous alkaline bath containing NaOH (5 g L^{-1}), $Na_2CO_3 \cdot 6H_2O$ (5 g L^{-1}), $Na_3PO_4 \cdot 12H_2O$ (10 g L^{-1}), $Na_2SiO_3 \cdot 5H_2O$ (1 g L^{-1}), and sodium gluconate ($NaC_6H_{11}O_7$, 10 g L^{-1}), then etched with aqueous NaOH (25 g L^{-1}) for one minute and neutralised with aqueous HNO_3 (ϕ_r = 20 %) for 2 min. The samples were rinsed with distilled water immediately after each step, carried out at ambient temperature.

The aluminium sheet was then used as anode and a lead plate (3 mm × 40 mm × 40 mm) as counter-electrode in the electrochemical cell with the thermostat at 25 ℃. The anodisation was run in potentiostatic mode (U_a = const.) using three different electrolytic aqueous baths (Zamora et al., 2004), all free of chromium species: (*i*) H_3PO_4 (78 g L^{-1}, pH 1.0) at 25 ℃; (*ii*) $Na_2B_4O_7$ (30 g L^{-1}, pH 9.3) at 65 ℃, and (*iii*) a mixed solution (pH 0.5) of H_2SO_4 (40 g L^{-1}) and H_3BO_3 (10 g L^{-1}) at 25 ℃. The voltage and anodisation time used for each electrolyte were typically 15 V for 15 min, 20 V for 20 min, and 20 V for 15 min, respectively. These experimental conditions were designated as the "standard conditions" of anodisation. Where different, the values of voltage or anodisation time are specified.

Nickel electro-deposition in the porous anodic films was performed in an electrochemical cell using the aqueous electrolytic baths previously developed by Salmi (2000) but with only phosphoric acid as anodisation electrolyte. The electrolyte was prepared from $NiSO_4 \cdot 6H_2O$ (30 g L^{-1}), H_3BO_3 (20 g L^{-1}), $MgSO_4 \cdot 7H_2O$ (20 g L^{-1}), and $(NH_4)_2SO_4$ (20 g L^{-1}). Prior to metal deposition, the sample was dipped in the electro-deposition electrolyte of (25 ± 2) ℃ for 30 s at open circuit voltage. Electrochemical deposition was then performed using (Blanc Electronique SA supply, type EA-4036, France) with a 50Hz alternating voltage; the voltage and current waveform were recorded by an oscilloscope. Deposition effective voltage and duration were typically 10 V and 600 s. After deposition, the specimens were removed from the electrolyte immediately and washed with de-ionised water.

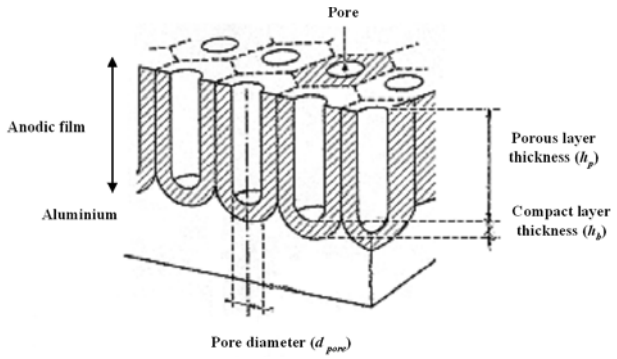

Fig. 1. Keller's model of the ideal microstructure of porous anodic film.

All chemicals used were of analytical grade (Prolabo, France) and aqueous electrolyte solutions were prepared using deionised water.

Following acid dissolution of the anodic film, chemical analysis of the deposited metal was performed by Inductively Coupled Plasma Optical Emission Spectrometry (ICP-OES) on a Jobin Yvon 24 spectrophotometer (Horiba, France). For this purpose, a disc (d = 14 mm) was cut in the treated zone of the sample and placed in an acid solution (10 mL of 0.1 M HNO_3) under vigorous mixing until the coating dissolved completely. The solution was then made up to a final volume of 50 mL with deionised water. Finally, the concentration obtained by ICP analysis was converted to nickel content per surface area (mg m^{-2}). Each experimental γ value is the average value of data from ICP measurements of three independent samples. In this case, the error is 5 %.

Transmission Electron Microscopy (TEM JEOL 200CX) (Horiba, France) was used to determine the morphology and the characteristics of the porous anodic film (Fig. 1), i.e. the pore density (ρ_{pores}), the pore diameter (d_{pore}) viewed from the TEM surface, and the height of the porous layer (h_p), the thickness of the barrier/compact layer (h_b) from the TEM cross-sectional view. Porosity (or void percentage) (τ) was calculated as: $\tau = \rho_{pores}(\pi/4)d_{pore}^2$. Following nickel electro-deposition, TEM was also used to determine the location of the metal and the average height of the deposited metal to calculate the theoretical value of the mass of deposited metal per unit area (γ).

Results and discussion

Control of characteristics of porous anodic films

The geometrical characteristics of the anodic films

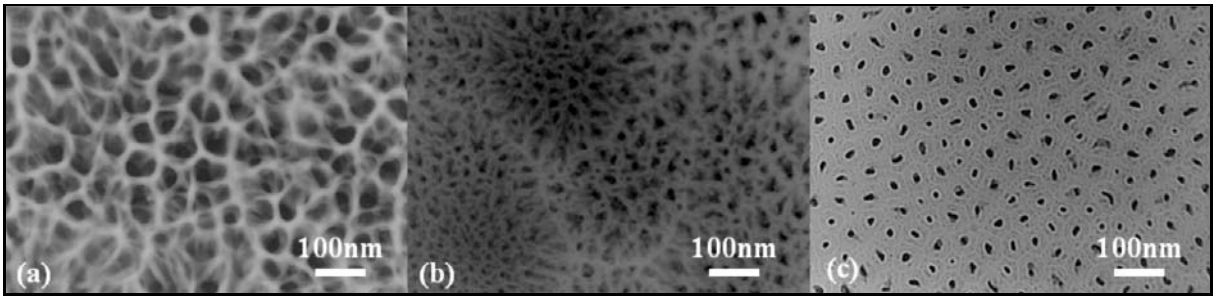

Fig. 2. TEM of surface of anodic films prepared in (a) phosphoric acid electrolyte, (b) borate electrolyte, (c) sulphuric acid–boric acid electrolyte.

Table 1. Correlations between anodisation voltage, anodisation electrolyte, and characteristics of anodic films

	Sulphuric–boric electrolyte	Phosphoric electrolyte	Borate electrolyte
Pore density/m^{-2}	$\rho_{\text{pores}} = 1.4 \times 10^{16} \frac{1}{U_a}$	$\rho_{\text{pores}} = 8.5 \times 10^{15} \frac{1}{U_a}$	–
Pore diameter/m	$d_{\text{pore}} = 1.5 \times 10^{-9} U_a + 9.2 \times 10^{-9}$	$d_{\text{pore}} = 3.1 \times 10^{-10} U_a + 5.5 \times 10^{-9}$	–
Height of porous layer, h_p/m	$h_p = 1.5 \times 10^{-7} e^{0.19 U_a}$	$h_p = 4.45 \times 10^{-8} U_a + 4.7 \times 10^{-8}$	$h_p = 3.3 \times 10^{-8} U_a + 5.6 \times 10^{-7}$
Height of barrier layer, h_b/nm	$h_b = 0.9 U_a$	$h_b = 1.12 U_a$	$h_b = 1.35 U_a$

were obtained in three different types of anodisation electrolytes. Firstly, typical TEM figures (Figs. 2a–2c) showed clear differences in microstructure depending on the electrolyte used.

The surface of the anodic films obtained in sulphuric–boric electrolyte was homogeneous and with a low porosity (4 %), composed of quasi-hexagonal cells, similar to those of Keller's model (Keller et al., 1953). The two other types of surfaces were more uneven and porous, i.e. showing 37 % and 12 % porosity for phosphoric and borate electrolytes, respectively.

The anodisation voltage and duration were then studied to establish correlations between the morphological characteristics of the anodic films, especially the porosity and the preparation conditions or operational parameters.

Impact of the anodising voltage

Anodising was performed in a fixed time and with a voltage varying between 5 V and 30 V. Pore density and average pore number were plotted against voltage for the different anodic film types in Figs. A1 and A2 (Appendix) while Figs. A3 and A4 plot the thickness of the porous and the compact layers. The correlations established for each of these characteristics according to the electrolyte used are summarised in Table 1.

These results clearly show that the pore diameter and thickness of the barrier layer were linearly dependent on the anodisation voltage under these experimental conditions. The proportionality between h_b and U_a is in agreement with previous works by Van der Linden et al. (1990). Moreover, the growth rate of the compact layer, i.e. the slope between h_b and U_a, obtained in the present study (from 0.90 nm V^{-1} to 1.35 nm V^{-1} (Table 1)) is comparable with the literature data (1.10 nm V^{-1} for sulphuric acid at 10 °C and 1.19 nm V^{-1} for phosphoric acid (Safrany, 2009; Trompette et al., 2010)). Concerning the thickness of the porous layer, the correlation also appeared linear for the phosphoric and borate electrolytes, but exponential for the sulphuric-boric electrolyte.

Impact of anodisation time

The influence of the anodisation time (t_a) was studied within the 300–1500 s range just for the sulphuric-boric electrolyte and a constant anodisation voltage (20 V). Figs A-5–A-8 show the changes of the geometrical parameters (ρ_{pores}, d_{pore}, h_p, h_b). Within the time range considered, the correlations were linear, except for pore density (Table 2). The thicknesses (h_p, h_b) were directly proportional to the time and the current density, in agreement with Faraday's law (Goueffon et al., 2010), while porosity, especially the pore diameter (d_p), increased with the time and thus with film thickness. By contrast, the changes in pore density were more unexpected and, as yet, unexplained.

Characteristics under standard conditions of anodisation

The morphological characteristics obtained under standard experimental conditions are summarised in

Table 2. Correlations between anodisation time (t_a) and characteristics of the anodic films; anodisation was performed in sulphuric–boric electrolyte at 20 V

Pore density/m^{-2}	$\rho_{pores} = 1.8 \times 10^{16} \frac{1}{\sqrt{t_a}}$
Pore diameter/m	$d_{pore} = 2.45 \times 10^{-12} t_a + 8.6 \times 10^{-9}$
Height of porous layer, h_p/m	$h_p = 4.6 \times 10^{-9} t_a + 8.8 \times 10^{-7}$
Height of barrier layer, h_b/nm	$h_b = 7 \times 10^{-3} t_a + 26.3$

Table 3. Characteristics of the anodic films obtained under standard experimental conditions

Electrolyte	Sulphuric–boric	Phosphoric	Borate
Conditions	15 min, 20 V, 25 °C	15 min, 15 V, 25 °C	20 min, 20 V, 65 °C
Pore density/m^{-2}	$(5.4 \pm 0.2) \times 10^{14}$	$(5.2 \pm 0.8) \times 10^{14}$	$(15 \pm 2) \times 10^{14}$
Pore diameter/nm	10 ± 4	30 ± 9	10 ± 4
Height of porous layer/μm	6.1 ± 0.2	0.69 ± 0.03	1.56 ± 0.02
Height of barrier layer/nm	19 ± 3	18 ± 1	21 ± 2
τ/(m^2 m^{-2})	0.04	0.37	0.12
Percentage of void surface per sample surface/%	4	37	12

Table 3, the present values being in agreement with previous works. The pore density was $(5.4 \pm 0.2) \times 10^{14}$ m^{-2} and $(5.2 \pm 0.8) \times 10^{14}$ m^{-2} for the sulphuric–boric and phosphoric electrolytes respectively, while previous results were in the range of 2.8×10^{14} m^{-2} to 7.6×10^{14} m^{-2} (sulphuric acid–boric acid) and 1.9×10^{14} m^{-2} (phosphoric acid) (Safrany, 2008). The thicknesses of the barrier layer obtained for the three electrolytes were also similar to those obtained by Dasquet et al. (2000b). By contrast, the greatest difference concerned the total thickness of the porous layer, although identical electrolytes were used. However, this characteristic depends on several parameters, especially on the initial voltage slope, to reach the nominal value.

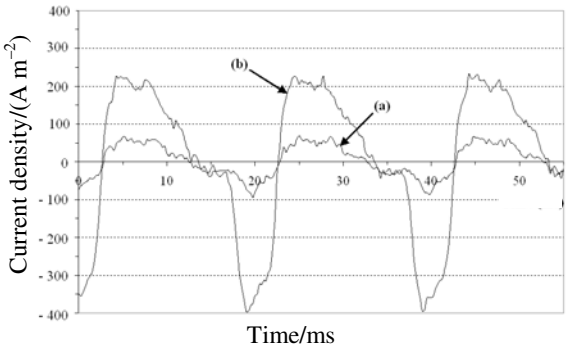

Fig. 3. Comparison of current density waveforms obtained during nickel electro-deposition (10 V, 5 s) using anodic films prepared in (a) mixed sulphuric–boric acid solution (20 V, 15 min) and (b) phosphoric acid solution (15 V, 15 min).

Electrical behaviour during electro-deposition: Repeatability and anodic film impact

With a view to checking the repeatability of the process, current densities were recorded during two nickel electro-deposition experiments, using the same type of anodic film prepared (20 V, 900 s) in the sulphuric–boric bath. The results highlight that the curves are identical in the 5–600 s time range; this was also true for each of the other two types of anodic films. Hence, the results clearly confirm that the electro-deposition step is repeatable.

Additional experiments were carried out under the same conditions of Ni deposition (10 V, 5 s) but with the three different anodic films. There were no differences from a qualitative point of view, but the amplitude of the current density wave changed. It can be seen, for example, that the intensities corresponding to the phosphoric anodic film were higher than those related to the sulphuric–boric electrolyte (Fig. 3). This result cannot be explained here by a difference in the barrier layer thickness (Table 3), but probably by the different porosities of the anodic films, 37 % and 4 % respectively.

Impact of duration of electro-deposition

Current density variations were also recorded at different times (Fig. 4) during nickel deposition (10 V) using an anodic film from sulphuric-boric solution (20 V, 900 s). As in results reported previously (Dasquet et al, 2000a) concerning zinc electro-deposition, the current density waveform was asymmetric and then clearly decreased for both the anodic and cathodic parts at the beginning of the deposition experiment.

For duration longer than 420 s, this electrical signal became constant, with no further changes. Similar

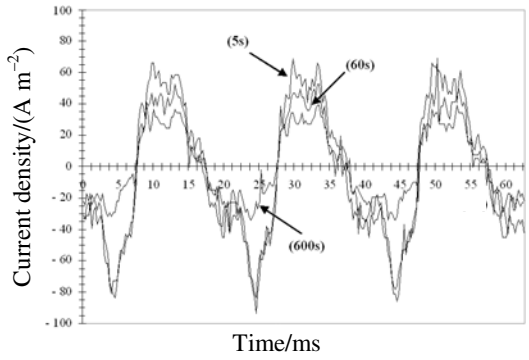

Fig. 4. Current density waveforms as a function of time (5 s, 60 s, 600 s) of Ni deposition at 10 V using an anodic film from sulphuric–boric electrolyte (20 V, 900 s).

results were observed for the two other anodic films. However, at lower voltages, for example 7 V for Ni deposition, the current density curve did not change at all, irrespective of the deposition time. This unusual behaviour at low voltage was observed when anodic films were produced in phosphoric or borate solutions.

The voltage impact was previously explained (Arurault et al., 2010) for nickel electro-deposition after anodising in sulphuric–boric electrolyte: it depends on the voltage applied in comparison with the threshold voltage U_t. For lower values (here 7 V), the coating acts only as a capacitor, while at higher voltages (here 10 V), both the anodic and cathodic parts of the current waveform change with the deposition time. At the higher voltage, additional oxidation of the aluminium substrate occurred during the anodic part of the waveform, because of the semi-conducting characteristics of the barrier layer, while metal deposition (and solvent reduction) occurred during the cathodic part. This difference in the reactions explains the asymmetry of the current density waveform at the beginning of the electro-deposition step. When the over-oxidation of the aluminium substrate is completed, the electri-

Table 4. Characteristics of the anodic films prior and after metal deposition and experimental data (from ICP-OES analyses) and calculated values (from TEM observations) of metal deposited

Anodisation electrolyte, deposition		Thickness of porous layer	Average diameter of pores	Height of barrier layer	Average height of metal deposited	γ	
						experimental (5 % error)	calculated
		μm	nm	nm	nm	mg m^{-2}	
Sulphuric acid–boric acid mixed solution	Before	6.1 ± 0.2	10 ± 4	19 ± 3	–	–	–
	After	2.0 ± 0.1	8 ± 3	27 ± 3	500 ± 100	147	189
Phosphoric acid solution	Before	0.7 ± 0.3	30 ± 9	18 ± 1	–	–	–
	After	0.8 ± 0.2	38 ± 10	30 ± 2	60 ± 5	583	196
Borate solution	Before	1.6 ± 0.1	10 ± 4	21 ± 2	–	–	–
	After	1.1 ± 0.1	11 ± 4	30 ± 4	70 ± 10	364	74

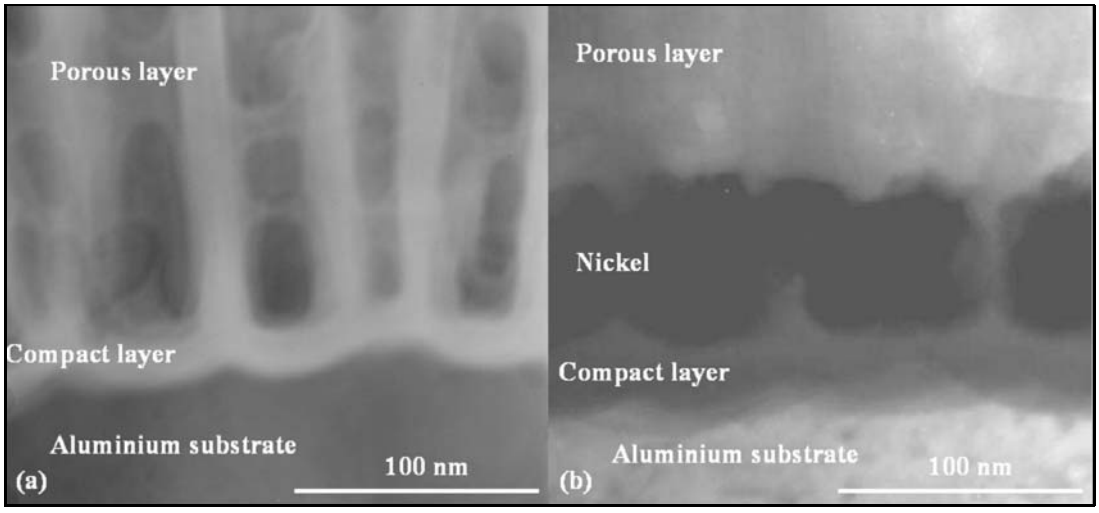

Fig. 5. TEM cross-sectional view of the phosphoric anodic film (15 V, 15 min) (a) before and (b) after nickel electro-deposition (10 V, 600 s).

cal behaviour depends only on the thick new compact layer during both the positive and negative parts of the alternating voltage applied: the current density waveform becomes symmetrical and metal is no longer deposited.

Characteristics of the anodic films containing metal: Morphological characteristics

The microstructure obtained by TEM after nickel deposition (10 V, 600 s) in a film anodised in phosphoric solution is illustrated in Fig. 5. Values characterising the morphology of the three types of anodic film impregnated with nickel are given in Table 4.

Porous film structure did not change: pore density and diameter did not vary significantly with the insertion of metal in the anodic film under alternating voltage conditions, whereas the barrier layer thickness increased irrespective of the anodic film used. Furthermore, for the three types of anodic films, final thickness was about 30 nm after deposition treatment at an effective alternating voltage of 10 V.

The increase in barrier layer thickness during the deposition process confirms experimentally the hypothesis of further anodisation of the substrate during the anodic part of the alternating signal. This explanation is supported by the identical thickness (about 30 nm) obtained for the final barrier layer, regardless of the anodisation conditions (electrolyte, duration, voltage). This thickness is largely dependent on the peak value (14 V) of the deposition voltage, especially in its anodic part. To check this hypothesis, the barrier layer thickness could be measured as a function of voltage applied.

Moreover, no variation in the porous layer thickness occurred for the film anodised in phosphoric solution, whereas a decrease was observed for the films anodised in sulphuric–boric and borate solutions, suggesting that the porous layer was occasionally partially dissolved during the deposition process.

TEM observations also revealed two additional points: the metal was located at the bottom of the pores, in contact with the barrier layer, and metal height in the porous layer was irregular. These two results remain valid for all three types of anodic film. The location of the metal at the bottom of the pores is in agreement with previous works (Shaffei et al., 2001) and can be explained by the low electrical resistivity of the anodic film at these points. The irregular height of metal, sometimes called the "sky-scraper" phenomenon (Yin et al., 2001), is usually explained by irregularities in the compact layer thickness along the aluminium substrate interface.

Metal content

The metal content γ introduced into the pores of the three different types of anodic films for the same nickel deposition treatment (10 V, 600 s) is reported in Table 4. The nature of the anodic film appears to play a significant role in the quantity of metal deposited. In fact, this value increased four-fold (from 0.147 g m^{-2} to 0.583 g m^{-2}) between anodisation carried out in sulphuric–boric and in phosphoric electrolytes, respectively. In addition, these values are in accordance with the previous results by Granqvist et al. (1979) reporting nickel contents from 0.5 g m^{-2} to 1 g m^{-2} depending on the operational conditions of metal deposition. These results can be explained by differences in the porosities. In particular, the highest amount of nickel (583 mg m^{-2}) corresponds to the highest porosity (37 %), while the lowest value (147 mg m^{-2}) is linked to the lowest void fraction (4 %).

By making some assumptions it is then possible to calculate the theoretical mass of metal deposited in the porous anodic film, and then to compare this theoretical value with the experimental data obtained from ICP analyses after film dissolution. Assuming that the pore density here is unchanged by metal deposition, the density of deposited metal is almost equal to the density of pure metal (ρ_{Ni} = 8.9 g cm^{-3}), while the average pore diameter and the representative average height (h_{Ni}) of metal deposited can be determined by TEM observations.

Therefore, the mass of metal deposited per unit area (γ) (Eq. (1)) can be calculated from the volume of metal deposited (V_{Ni}) in the pores (Eq. (2)) and also from the pore density ρ_{pores} and the nickel density d_{Ni} as:

$$\gamma = V_{Ni}\rho_{pores}d_{Ni} \quad (1)$$

$$V_{Ni} = \left(\frac{\pi}{4}d_{pore}^2\right)h_{Ni} \quad (2)$$

For anodic films from sulphuric–boric solution, the calculated and experimental quantities of nickel were similar (Table 4), whereas for the phosphoric and borate anodic films, the difference between calculated and experimental values was 3- to 5-fold. These results could be explained initially by differences between the densities of metal and oxide, causing differences in calculated and experimental quantities of metal. But Goad and Moskovits (1978) demonstrated that nickel deposited was present solely as metal inside the anodic films, when alternating voltage was used.

The second explanation is based on the possible alteration of the height of metal in the pores, due to sample preparation, especially ion thinning for the TEM observations. Moreover, partial re-oxidation of the metal deposited could also be considered. Hence, the theoretical value would be substantially underestimated. Additional experiments would be required to provide an unambiguous explanation for these differences.

The impact of the deposition time on the quantity of metal deposited was then studied for nickel (10 V, 600 s) in anodic films from sulphuric–boric solution

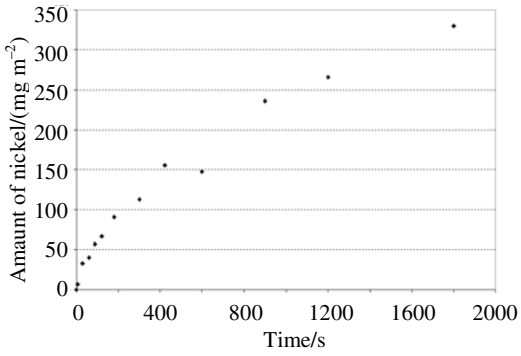

Fig. 6. Amount of nickel in anodic films from sulphuric–boric electrolyte (10 V, 900 s) vs. the duration of electrodeposition (10 V).

(20 V, 900 s). The quantity of metal deposited versus the deposition time (Fig. 6) is in agreement with previous works involving zinc (Dasquet et al., 2000a): a strong increase for short times (less than 180 s) then a slower increase. This inflexion has previously been explained (Dasquet et al., 2000a) by the partial electrochemical redissolution that occurs during the anodic part of the alternating voltage waveform. Furthermore, it was previously claimed (Arurault & Bes, 2003) that the $\gamma = f(t)$ variation could be described by a mathematical Elovich-type law (Eq. (3)) in the 540–720 s time range. The fitting with the experimental data here appears to be satisfactory for the deposition times tested (up to 1800 s), longer than the deposition time previously considered (Arurault & Bes, 2003). Thus, the values of the constants are $A = 4.55 \times 10^{-3}$ s^{-1} and $B = 140$ mg m^{-2} for nickel deposition in anodic films from sulphuric–boric electrolyte

$$\gamma = B \ln(1 + At_i) \tag{3}$$

Conclusions

The characteristics of porous anodic films were first studied as a function of the type of anodisation electrolyte used, the voltage and the duration. Experimental correlations showed that it was possible to control these characteristics, especially porosity. Then, nickel was deposited under alternating voltage. The impact of the anodic film on the current density waveforms and the metal content was mainly accounted for by porosity differences. Moreover, an increased deposition time led to over-oxidation of the aluminium substrate, experimentally highlighted by TEM, occurring during the positive part of the alternating waveform. The reduction during the negative part allowed for the deposition of nickel at the bottom of the pores. Various explanations are proposed to account for the differences between the experimental and calculated nickel contents. Finally, the impact of the deposition time on the quantity of metal laid down was successfully matched by using an Elovich type law over a large time span (up to 1800 s), demonstrating the ability to satisfactorily control the metal content, in order to prepare, for example – coloured coatings.

Appendix

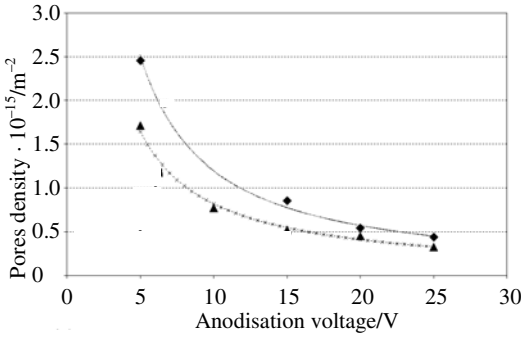

Fig. A1. Pore density vs. anodisation voltage for sulphuric–boric (◆) and phosphoric (▲) electrolytes (anodisation time: 15 min).

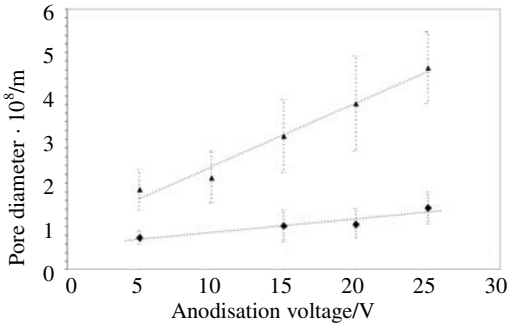

Fig. A2. Pore diameter vs. anodisation voltage for sulphuric–boric (◆) and phosphoric (▲) electrolytes (anodisation time: 15 min).

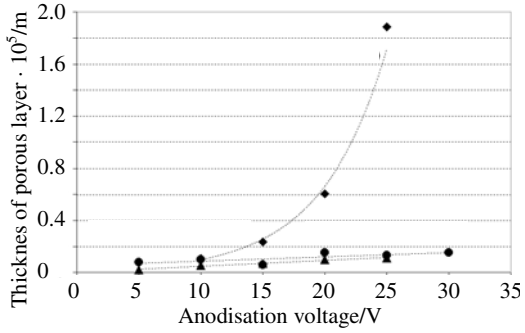

Fig. A3. Thickness of porous layer vs. anodisation voltage for sulphuric–boric (◆), phosphoric (▲), and boric (●) electrolytes (anodisation time: 15 min, for the borate electrolyte 20 min).

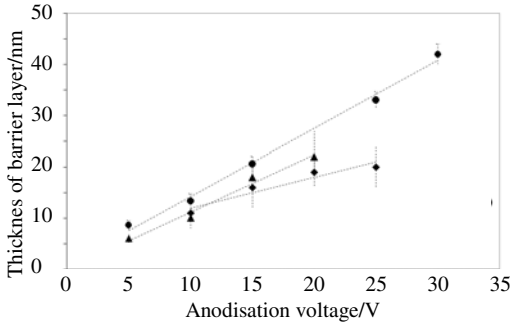

Fig. A4. Thickness of barrier layer vs. anodisation voltage for sulphuric–boric (◆), phosphoric (▲), and boric (●) electrolytes (anodisation time: 15 min, for the borate electrolyte 20 min).

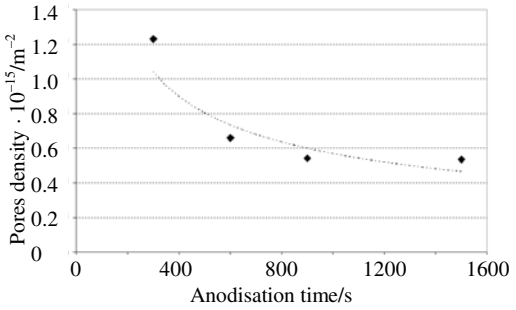

Fig. A5. Pore density vs. duration of anodisation for anodic films from sulphuric–boric electrolyte (20 V).

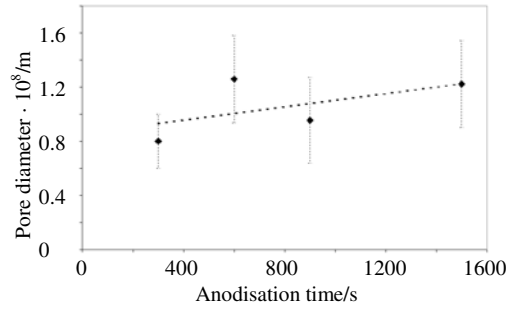

Fig. A6. Pore diameter vs. duration of anodisation for anodic films from sulphuric–boric electrolyte (20 V).

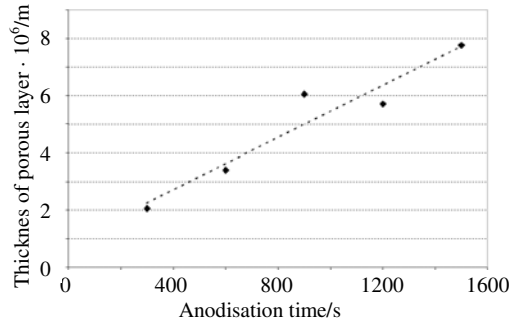

Fig. A7. Thickness of porous layer vs. duration of anodisation for anodic films from sulphuric–boric electrolyte (20 V).

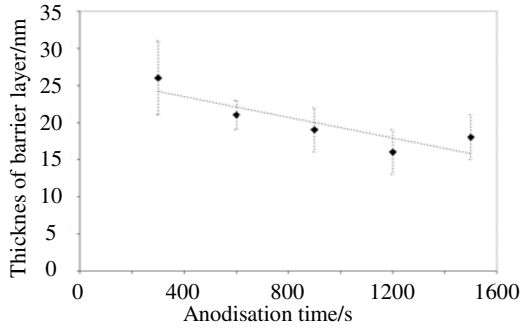

Fig. A8. Thickness of barrier layer vs. duration of anodisation for anodic films from sulphuric–boric electrolyte (20 V).

References

Anderson, Å., Hunderi, O., & Granqvist, C. G. (1980). Nickel pigmented anodic aluminium oxide for selective absorption of solar energy. *Journal of Applied Physics*, *51*, 754–764. DOI: 10.1063/1.327337.

Arurault, L., & Bes, R. S. (2007). Formulation de nouveaux bains pour la coloration électrolytique. *Galvano Organo Traitements de Surface*, *767*, 40–42.

Arurault, L., & Bes, R. S. (2003). Kinetics of metallic electrochemical impregnation of porous anodic oxidation layer on 1050 and 2024 aluminium alloys. *Advanced Engineering Materials*, *5*, 433–435. DOI: 10.1002/adem.200300252.

Arurault, L., Salmi, J., & Bes, R. S. (2004). Comparison of AC voltage and periodic-reverse current nickel pigmented anodized aluminium as solar selective absorber. *Solar Energy Materials and Solar Cells*, *82*, 447–455. DOI: 10.1016/j.solmat.2004.02.002.

Arurault, L., Zamora, G., & Bes, R. S. (2006). Energetic costs of the electrochemical steps during the preparation of aluminium porous anodic layers impregnated by metals. *ATB Métallurgie*, *45*, 306–309.

Arurault, L., Zamora, G., Vilar, V., Winterton, P., & Bes, R. (2010). Electrical behaviour, characteristics and properties of anodic aluminium oxide films coloured by nickel electrodeposition. *Journal of Material Science*, *45*, 2611–2618. DOI: 10.1007/s10853-010-4235-8.

Chi, G. J., Yao, S. W., Fan, J., Zhang, W. G., & Wang, H. Z. (2002). Antibacterial activity of anodized aluminium with deposited silver. *Surface and Coatings Technology*, *157*, 162–165. DOI: 10.1016/S0257-8972(02)00150-0.

Dasquet, J.-P., Bonino, J.-P., Caillard, D., & Bes, R. S. (2000a). Zinc impregnation of the anodic oxidation layer of 1050 and 2024 aluminium alloys. *Journal of Applied Electrochemistry*, *30*, 845–853. DOI: 10.1023/A:1003947800813.

Dasquet, J.-P., Caillard, D., Conforto, E., Bonino, J.-P., & Bes, R. (2000b). Investigation of the anodic oxide layer on 1050 and 2024T3 aluminium alloys by electron microscopy and electrochemical impedance spectroscopy. *Thin Solid Films*, *371*, 183–190. DOI: 10.1016/S0040-6090(00)01016-6.

Forrer, P., Schlottig, F., Siegenthaler, H., & Textor, M. (2000). Electrochemical preparation and surface properties of gold nanowire arrays formed by the template technique. *Journal of Applied Electrochemistry*, *30*, 533–541. DOI: 10.1023/A:1003941129560.

Fukuda, Y., & Fukushima, T. (1982). Electrodeposition of nickel and zinc into the pores of anodic oxide film on aluminium. *Journal of the Metal Finishing Society of Japan*, *33*, 50–55.

Goueffon, Y., Arurault, L., Fontorbes, S., Mabru, C., Tonon, C., & Guigue, P. (2010). Chemical characteristics, mechanical and thermo-optical properties of black anodic films prepared on 7175 aluminium alloy for space applications. *Materials Chemistry and Physics*, *120*, 636–642. DOI: 10.1016/j.matchemphys.2009.12.016.

Granqvist, C. G., Andersson, Å., & Hunderi, O. (1979). Spectrally selective surfaces of Ni-pigmented anodic Al_2O_3. *Applied Physics Letters*, *35*, 268–270. DOI: 10.1063/1.91078.

Goad, D. G. W., & Moskovits, M. (1978). Colloidal metal in aluminium-oxide. *Journal of Applied Physics*, *49*, 2929–2934. DOI: 10.1063/1.325153.

Hwang, S.-K., Lee, J., Jeong, S.-H., Lee, P.-S., & Lee, K.-H. (2005). Fabrication of carbon nanotube emitters in an anodic aluminium oxide nanotemplate on a Si wafer by multi-step anodisation. *Nanotechnology*, *16*, 850–858. DOI: 10.1088/0957-4484/16/6/040.

Jagminas, A., Lichušina, S., Kurtinaitiené, M., & Selskis, A. (2003). Concentration effect of the solutions for alumina template ac filling by metals arrays. *Applied Surface Science*, *211*, 194–202. DOI: 10.1016/S0169-4332(03)00247-2.

Kallithrakas-Kontos, N., Moshohoritou, R., Ninni, V., & Tsangaraki-Kaplanoglou, I. (1998). Investigation of the relationship between the reflectance and the deposited nickel and tin amount on the aluminium anodic oxide film. *Thin Solid Films*, *326*, 166–170. DOI: 10.1016/S0040-6090(98)00569-0.

Kawai, S., & Ueda, R. (1975). Magnetic properties of anodic oxide coatings on aluminium containing electrodeposited Co and Co-Ni. *Journal of the Electrochemical Society*, *122*, 32–36. DOI: 10.1149/1.2134152.

Keller, F., Hunter, M. S., & Robinson, D. L. (1953). Structural features of oxide coatings on aluminum. *Journal of the Electrochemical Society*, *100*, 411–419. DOI: 10.1149/1.2781142.

Kyotani, T., Tsai, L.-f., & Tomita, A. (1996). Preparation of ultrafine carbon tubes in nanochannels of an anodic aluminium oxide film. *Chemistry of Materials*, *8*, 2109–2113. DOI: 10.1021/cm960063+.

Lee, J. H., Lee, D. N., & Kang, I. K. (1978). Alternating current color anodisation of aluminium alloys. *Plating and Surface Finishing*, *1*, 40–44.

McBren, P. H., & Moskovits, M. (1987). A surface-enhaced Raman study of ethylene and oxygen interacting with supported silver catalysts. *Journal of Catalysis*, *103*, 188–199. DOI: 10.1016/0021-9517(87)90105-9.

Nielsch, K., Müller, F., Li, A.-P., & Gösele, U. (2000). Uniform nickel deposition into ordered alumina pores by pulsed electrodeposition. *Advanced Materials*, *12*, 582–586. DOI: 10.1002/(SICI)1521-4095(200004)12:8-582.

Papadopoulos, C., Chang, B. H., Yin, A. J., & Xu, J. M. (2002). Engineering carbon nanotube via template growth. *International Journal of Nanoscience*, *1*, 205–212. DOI: 10.1142/S0219581X02000188.

Preston, C. K., & Moskovits, M. (1993). Optical characterization of anodic aluminium oxide films containing electrochemically deposited metal particles. 1. Gold in phosphoric acid anodic aluminium oxide films. *The Journal of Physical Chemistry*, *97*, 8495–8503. DOI: 10.1021/j100134a019.

Safrany, J. S. (2008). Anodisation de l'aluminium et de ses alliages. *Techniques de l'Ingénieur*, *6*(COR 12), M1630v2/1–M1630v2/27.

Salmi, J., Bonino, J.-P., & Bes, R. S. (2000). Nickel pigmented anodized aluminium as solar selective absorbers. *Journal of Materials Science*, *35*, 1347–1351. DOI: 10.1023/A:10047738 21962.

Sauer, G., Brehm, G., Schneider, S., Nielsch, K., Wehrspohn, R. B., Choi, J., Hofmeister, H., & Gösele, U. (2002). Highly ordered monocrystalline silver nanowire arrays. *Journal of Applied Physics*, *91*, 3243–3247. DOI: 10.1063/1.1435830.

Shaffei, M. F., Abd El-Rehim, S. S., Shaaban, N. A., & Huisen, H. S. (2001). Electrolytic coloring of anodic aluminum for selective solar absorbing films: use of additives promoting color depth and rate. *Renewable Energy*, *23*, 489–495. DOI: 10.1016/S0960-1481(00)00129-4.

Szkutnik, P. D., Maximovitch, S., Chainet, E., Dalard, F., Saulig, K., Dijon, J., & Pantigny, P. (2006). Aluminium anodisation process including oxide barrier removal for nanotechnological applications. *ATB Métallurgie*, *45*, 116–119.

Trompette, J. L., Arurault, L., Fontorbes, S., & Massot, L. (2010). Influence of the anion specificity on the electrochemical corrosion of anodized aluminum substrates. *Electrochimica Acta*, *55*, 2901–2910. DOI: 10.1016/j.electacta.2009.12.063.

Van der Linden, B., Terryn, H., & Vereecken, J. (1990). Investigation of anodic aluminium oxide layers by electrochemical impedance spectroscopy. *Journal of Applied Electrochemistry*, *20*, 798–803. DOI: 10.1007/BF01094309.

Wang, Z., Su, Y.-K., & Li, H.-L. (2002). AFM study of gold nanowire array electrodeposited within anodic aluminium oxide template. *Applied Physics A: Materials Science & Processing*, *74*, 563–565. DOI: 10.1007/s003390100909.

Wernick, S., Pinner, R., & Sheasby, P. G. (1987). *The surface treatment and finishing of aluminum and its alloys* (5th ed.). Teddington, England: ASM International.

Wu, H.-Y., Zhao, Y., & Jiao, Q.-Z. (2009). Nanotube arrays of Zn/Co/Fe composite oxides assembled in porous anodic alumina and their magnetic properties. *Journal of Alloys Compounds*, *487*, 591–594. DOI: 10.1016/j.jallcom.2009.08.018.

Yang, S., Zhu, H., Yu, D., Jin, Z., Tang, S., & Du, Y. (2000). Preparation and magnetic property of Fe nanowire array, *Journal of Magnetism and Magnetic Materials*, *222*, 97–100. DOI: 10.1016/S0304-8853(00)00541-2.

Yin, A. J., Li, J., Jian, W., Bennett, A. J., & Xu, J. M. (2001). Fabrication of highly ordered metallic nanowire arrays by electrodeposition. *Applied Physics Letters*, *79*, 1039–1041. DOI: 10.1063/1.1389765.

Yoo, W.-C., & Lee, J.-K. (2004). Field-dependent growth patterns of metals electroplated in nanoporous alumina membranes. *Advanced Materials*, *16*, 1097–1101. DOI: 10.1002/adma.200306595.

Zamora, G., Arurault, L., & Bes, R. S. (2004). Aspectos energéticos y caracteristicas: De las capas anódicas porosas elaboradas en aleaciones de aluminio 1050A. *Pinturas y Acabados Industriales*, *46*(290), 36–40.

Zemanová, M., Chovancová, M., Blaho, P., Ušák, E., & Valtýni, J. (2008a). Effect of plating mode and complexing agent on morphology of pigmented anodic alumina coatings. *Transactions of the Institute of Metal Finishing*, *86*, 109–114. DOI: 10.1179/174591908X272933.

Zemanová, M., Chovancová, M., Gáliková, Z., & Krivošík, P. (2008b). Nickel electrolytic colouring of anodic alumina for selective solar absorbing films. *Renewable Energy*, *33*, 2303–2310. DOI: 10.1016/j.renene.2008.01.005.

Zemanová, M., Chovancová, M., & Krivošík, P. (2009a). A new approach to nickel electrolytic colouring of anodised aluminium. *Chemical Papers*, *63*, 62–70. DOI: 10.2478/s11696-008-0081-4.

Zemanová, M., Gál, M., & Chovancová, M. (2009b). Effect of frequency on pulse electrolytic colouring process of anodised aluminium. *Transactions of the Institute of Metal Finishing*, *87*, 97–101. DOI: 10.1179/174591909X424186.